

Reactions between cold methyl halide molecules and alkali-metal atoms

Jesse J. Lutz and Jeremy M. Hutson

Joint Quantum Centre (JQC) Durham-Newcastle, Department of Chemistry,
Durham University, South Road, Durham, DH1 3LE, United Kingdom

(Dated: August 10, 2018)

We investigate the potential energy surfaces and activation energies for reactions between methyl halide molecules CH_3X ($X = \text{F}, \text{Cl}, \text{Br}, \text{I}$) and alkali-metal atoms A ($A = \text{Li}, \text{Na}, \text{K}, \text{Rb}$) using high-level *ab initio* calculations. We examine the anisotropy of each intermolecular potential energy surface (PES) and the mechanism and energetics of the only available exothermic reaction pathway, $\text{CH}_3\text{X} + A \rightarrow \text{CH}_3 + \text{AX}$. The region of the transition state is explored using two-dimensional PES cuts and estimates of the activation energies are inferred. Nearly all combinations of methyl halide and alkali-metal atom have positive barrier heights, indicating that reactions at low temperatures will be slow.

I. INTRODUCTION

Recent improvements in experimental techniques for cooling gas-phase atoms and ions to cold ($T < 1$ K) and ultracold ($T < 1$ mK) temperatures have ushered in an exciting new era of low-energy structure and dynamics research. Interest has broadened to encompass neutral diatomic and polyatomic molecules, where fundamental applications are being pursued, including controlled ultracold chemistry,¹ quantum information and computing,² and high-precision measurements that place limits on the time-dependence of fundamental constants.³⁻⁵

Deceleration and trapping of molecules presents a more formidable challenge than for atoms, due to additional internal vibrational and rotational energy structure, enhanced long-range forces resulting from molecular multipole interactions, and the possibility of collision-induced chemical reactivity. In the cold regime, molecules exist primarily in their ground electronic and rovibrational states and long-range forces and resonance phenomena play a dominant role in the outcome of collisions.

The current approaches for producing ultracold molecules fall into two categories. First, there are *direct* methods for cooling, where molecules already in their desired chemical form are cooled from higher temperatures. Helium buffer-gas cooling,⁶ Stark deceleration,⁷ and Zeeman deceleration⁸⁻¹⁰ are the most widely used techniques of this kind, but laser cooling of SrF ¹¹ has also been reported. Opto-electrical cooling using the Sisyphus effect has also recently been demonstrated for electrically trapped CH_3F molecules.¹⁵ Secondly, there are *indirect* methods, where previously cooled atoms are combined by photoassociation^{16,17} or tuning across magnetic Feshbach resonances.^{16,18} While indirect methods have been applied with much success to produce ultracold alkali-metal dimers, direct methods are currently more generally applicable for other molecules.¹⁹⁻²⁵ The present lower limit for temperatures that may be accessed using direct methods is 10 to 100 mK, and as a result “second-stage” cooling techniques are needed to bridge the gap to gain entrance into the microkelvin regime.

Among the most promising second-stage cooling methods are *sympathetic cooling*,¹² whereby a thermally hot

species is cooled by immersion within a sample of another previously cooled species, and evaporative cooling¹³, where the hottest molecules are selectively removed from the sample. Sympathetic cooling requires thermalization to occur before molecules are lost from the trap. Magnetic and electrostatic traps rely on the atoms and molecules remaining in specific low-field seeking states resulting from the Zeeman and Stark splittings that exist in an applied field. Inelastic or reactive collisions that cause transitions away from these states convert internal energy into translational energy and result in ejection of both species from the trap. The major challenge is therefore to minimize inelastic and reactive collisions. If reactive collisions can be ruled out as energetically forbidden, then it is the ratio of elastic to inelastic cross sections that determines the likelihood of success of sympathetic cooling. Inelastic cross sections are often suppressed at low collision energies and fields by centrifugal barriers.¹⁴

Symmetric-top molecules have particular advantages for sympathetic cooling. They have near-first-order Stark effects, which allow them to be decelerated and trapped electrostatically and then brought into contact with a magnetically trapped coolant. The fact that the two species are trapped independently allows the clouds to be matched in size even when the temperatures are different. In particular, there has been extensive experimental and theoretical work on the collisions of NH_3 and ND_3 with Rb .²⁶⁻²⁸ Żuchowski and Hutson²⁶ explored the potential energy surfaces (PESs) for NH_3 interacting with alkali-metal and alkaline-earth atoms and found them all to be deep and strongly anisotropic. Among the potentials for interactions with easily coolable atoms, Rb-NH_3 was the least anisotropic, so this system was chosen for detailed collision calculations.²⁷ However, it was found that, even in the absence of an electric field, molecules that are initially in the upper (f) component of the tunneling doublet undergo fast inelastic transitions to the lower (e) component. Parazzoli *et al.*²⁸ subsequently carried out an experiment in which an electrostatic trap containing cold ND_3 was overlapped with a magnetic trap containing Rb , and observed inelastic collisions even faster than predicted; they also carried out collision calculations in an electric field, and demonstrated that the field could

cause substantial changes in the inelasticity.

One reason for the fast inelastic collisions involving ND_3 in its upper tunneling is that the kinetic energy release due to tunneling persists even at zero electric field. The tunneling splitting in ND_3 is 0.0534 cm^{-1} , which corresponds to a kinetic energy release of 77 mK. This is considerably higher than the centrifugal barriers so precludes the possibility of centrifugal suppression of inelasticity for low-energy collisions. This led us to consider whether other symmetric-top molecules without tunneling would be better candidates for sympathetic cooling. In this work we begin to investigate the prospect of sympathetic cooling of the methyl halides, CH_3X ($X = \text{F}, \text{Cl}, \text{Br}, \text{I}$) by alkali-metal atoms A ($A = \text{Li}, \text{Na}, \text{K}, \text{Rb}$). The methyl halides all have substantial dipole moments ($\mu = 1.858, 1.892, 1.822, 1.620 \text{ D}$, respectively) so are amenable to electrostatic deceleration and trapping.²⁹ However, there is a considerable class of reactions between alkali-metal atoms and halogen-containing molecules for which the reaction pathways are barrierless³⁰ or have barriers submerged beneath the energy of separated reactants. In the context of sympathetic cooling, it is crucial to rule out the possibility of fast reactions between the colliding species before considering nonreactive scattering phenomena.

Reactive collisions between CH_3X and A at cold and ultracold temperatures are likely only if the reactions are exothermic and are either barrierless or have submerged barriers. For the species of interest here, there is only one exothermic reaction pathway, a dissociative charge transfer (DCT) forming methyl radical and alkyl halide products: $\text{CH}_3\text{X} + A \rightarrow \text{CH}_3 + \text{AX}$. The primary goal of the present study is to determine whether activation barriers exist for this class of reactions.

Reactions between alkali-metal atoms and methyl halides have been studied intensively in the field of reaction dynamics. However, very few *ab initio* studies have pursued gas-phase activation barriers for these reactions. Chang *et al.*³¹ and Hudson *et al.*³² studied ground-state and excited-state potential energy surfaces for $\text{Li} + \text{CH}_3\text{F}$ and $\text{Na} + \text{CH}_3\text{X}$ ($X = \text{F}, \text{Cl}, \text{Br}$), respectively, but focused on the regions around the global minima. They did not characterize transition states and indeed they did not find the surfaces that are important for the reactions: evidently the reactive surfaces correspond to high-lying excited states at near-equilibrium geometries and fall rapidly in energy as the C-X bond is stretched. We could not find in the literature any study which located transition states for the DCT reactions.

Thorough *ab initio* studies do exist modeling the related dissociative electron attachment (DEA) reactions, $\text{CH}_3\text{X} + e^- \rightarrow \text{CH}_3 + \text{X}^-$, for CH_3F ,^{33–36} CH_3Cl ,^{33,34,37,38} and the remaining methyl halides.^{33,35,39} Wu³³ proposed that $\text{CH}_3\text{X} + A$ DCT reactions could be modeled by their analogous $\text{CH}_3 + e^-$ DEA processes. In his work the alkali-metal atom was approximated by a free electron and the competing neutral and anionic potential energy curves along the C-X bond-breaking coordinate were constructed

semi-empirically. These two curves cross at a point whose energy can be viewed as the activation energy for the DEA reaction. This activation energy was found to have a strong dependence on the identity of the halogen, with the predicted values decreasing from 1.90 eV for CH_3F to 0.026 eV for CH_3I . Polarization and steric effects due to the presence of the alkali-metal are however a major concern in the DCT systems and it is questionable whether accurate reaction energetics can be obtained within this approximation. On the other hand, it is useful to understand when such approximations are valid, since simple models are computationally less taxing than the conventional supermolecular approach.

The effect of the direction of approach on reactive collisions of alkali-metal atoms with symmetric-top molecules has been explored experimentally. The groups of Brooks,^{40–44} Bernstein,^{45–50} and Stolte^{51–55} oriented molecules in hexapole electric fields, while the group of Loesch oriented them in high static electric fields.⁵⁶ This work helped classify the $\text{CH}_3\text{I} + A$ DCT reactions as “rebound” reactions, initiated by a close, orientation-dependent approach of the alkali-metal atom, where one reactant must hit the other more-or-less head-on for reaction to occur. There is a strong propensity for backward scattering of the alkyl halide product. This dependence of the probability of electron transfer on the molecular orientation is characterized by the “acceptance angle”; see Ref. 57 for a review.

Wiskerke *et al.*⁵⁸ revisited the experiments on the $\text{CH}_3\text{I} + \text{K} \rightarrow \text{CH}_3 + \text{KI}$ reaction more recently. They argued that the reaction is more likely to proceed if the collision time is comparable to or longer than the time required for the C-I bond to stretch. They concluded their study by calling for further theoretical examination of (1) the extent to which the CH_3I symmetric stretch is coupled to the relative motion in the entrance valley, (2) the topology of the seam between the covalent and ionic potentials, and (3) the general mechanism whereby CH_3I comes to act as a charge receptor.

The present work is motivated both by interest in cold molecular collisions and by the theoretical questions regarding the mechanism and energetics of the $\text{CH}_3\text{X} + A$ DCT reactions. We perform calculations that explicitly model the approach of the alkali-metal atom in order to obtain an approximate activation barrier for the reaction pathway of each system. This paper is structured as follows: In Sec. II we introduce the computational methods applied throughout the study. In Sec. III A we consider nonreactive intermolecular potentials, characterizing important stationary points and comparing anisotropies. Having established the most favorable intermolecular orientation for reaction, we then investigate the topology of the ground-state reactive PES in Sec. III B. In Sec. III C we explore minimum-energy reaction profiles and estimate the activation energy for each system. Finally, in Sec. IV we summarize the implications of the results in the context of sympathetic cooling and suggest particularly promising sympathetic cooling partners upon which

to focus in future work.

II. COMPUTATIONAL METHODS

The interaction energy of two monomers A and B is defined as $E_{\text{int}}^{AB} = E^{AB} - E^A - E^B$, where E^{AB} is the energy of the dimer and E^A and E^B are the energies of the isolated monomers. For potential energy surfaces between rigid monomers, we use the single-reference coupled-cluster (CC) method including single and double excitations and a noniterative treatment of triple excitations, abbreviated as CCSD(T). In particular, we use the partially spin-restricted open-shell CCSD(T) method, RCCSD(T),^{59,60} because it offers a highly accurate treatment of dynamical correlation at a relatively low computational cost, while avoiding potential spin-contamination issues often associated with unrestricted variants. All correlation energy calculations in this study were performed with core orbitals kept frozen.

The RCCSD(T) method can produce divergent energetics when nondynamical correlation effects become important, which can occur for stretched nuclear configurations. One solution to this is to use multireference approaches such as the complete-active-space self-consistent field (CASSCF) method, which always gives qualitatively correct energetics for reactive surfaces, provided the active space is adequately large.^{61,62} In the present work, we use CASSCF calculations with 11 electrons distributed among 10 orbitals, designated (11,10); these orbitals correspond asymptotically to the valence s and p shells of the alkali-metal atom and the two higher-lying A' and the two E valence molecular orbitals of CH_3X .

The CASSCF approach does not provide accurate relative energetics and can produce artificial transition states if the active space is inadequate; see Ref. 63 for a recent example. Many of the shortcomings associated with CASSCF may be overcome by applying a multi-state multi-reference second-order perturbation theory treatment of the correlation energy (MS-MR-CASPT2) on top of a state-averaged CASSCF reference.^{64,65} When employing the more expensive MS-MR-CASPT2 approach, we use a smaller and computationally more tractable (3,6) active space, which differs from the (11,10) active space by the omission of the two valence CH_3X molecular orbitals of E symmetry. A level shift of 0.2 was also applied to avoid intruder state problems.⁶⁶

Another method which has been shown to provide accurate relative energetics for potential energy surfaces involving cleavage of a single bond is the rigorously size-extensive completely renormalized CC method with singles, doubles, and non-iterative triples, referred to as CR-CC(2,3).⁶⁷⁻⁷⁰ This method has been shown to be as accurate as RCCSD(T) in situations where the latter performs well,^{71,72} while succeeding in a few specific cases where RCCSD(T) fails, such as for single-bond breaking.^{73,74} When computing reaction barrier heights, experience has

shown that when CCSD(T) and CR-CC(2,3) agree, both faithfully reproduce full CCSDT results.^{71,72} Thus, in this work we use the CR-CC(2,3) method as a diagnostic tool for testing the accuracy of CCSD(T).

First-, second- and third-row atoms are described using Dunning’s $cc\text{-pV}xZ$ or $aug\text{-cc-pV}xZ$ basis sets^{75,76} (where x is the cardinal number of the basis set), abbreviated throughout as VxZ or $AVxZ$, respectively. Where Dunning’s basis sets are too large to be computationally tractable, Pople’s 6-31G* basis sets⁷⁷⁻⁸⁰ are used instead. We use the Stuttgart ECP10MDF pseudopotentials (PPs) for K and Br and the ECP28MDF PPs for Rb and I.⁸¹⁻⁸³ We use the usual complementary basis sets for K and Rb⁸¹ and the ECP10MDF_AV xZ ⁸² and ECP28MDF_AV xZ PPs basis sets for Br and I, respectively; the cardinal number x is chosen to match that for the all-electron VxZ or $AVxZ$ basis sets used for the other atoms in the same calculation.

Some regions of the potential energy surfaces computed here are dominated by van der Waals forces. The representation of the dispersion energy is greatly improved by inclusion of midbond functions and elimination of basis set superposition error. For nonreactive surfaces, we include midbond functions with exponents sp : 0.9, 0.3, 0.1 for the AVDZ basis set and, additionally, df : 0.6, 0.2 for the AVTZ basis set and correct for basis-set superposition error using the counterpoise correction.⁸⁴ For reactive surfaces, we use results from calculations without counterpoise corrections because they can sometimes worsen results in such situations.⁸⁵

In this work, single-point energy calculations are often preceded by geometry optimizations, allowing secondary geometrical parameters to relax in response to those explicitly varied. As an example, an optimization using restricted second-order Møller-Plesset perturbation theory (RMP2) with the AVDZ basis set and followed by an RCCSD(T) single-point energy calculation using the AVTZ basis set is designated by the abbreviation MP2/AVDZ//RCCSD(T)/AVTZ. If the two basis sets are identical, only one is given.

The geometrical parameters that are always allowed to vary during optimizations are the C-H internuclear distance R_{CH} , the X-C-H bond angle θ_{XCH} , and, where applicable, the A-X internuclear distance R_{AX} and the X-C-A bond angle, θ_{XCA} . Unless otherwise noted, the CH_3X fragment is always restricted to C_{3v} symmetry and the A fragment is constrained to approach from a H-C-X-A torsion angle of $\phi = 180^\circ$.

The RMP2, RCCSD(T), CASSCF, and MS-MR-CASPT2 calculations were performed with MOLPRO⁸⁶ and CR-CC(2,3) calculations were performed using GAMESS.^{87,88} Basis sets and PPs were retrieved from the EMSL basis set exchange⁸⁹ and Stuttgart/Cologne Group PP repository,⁹⁰ respectively.

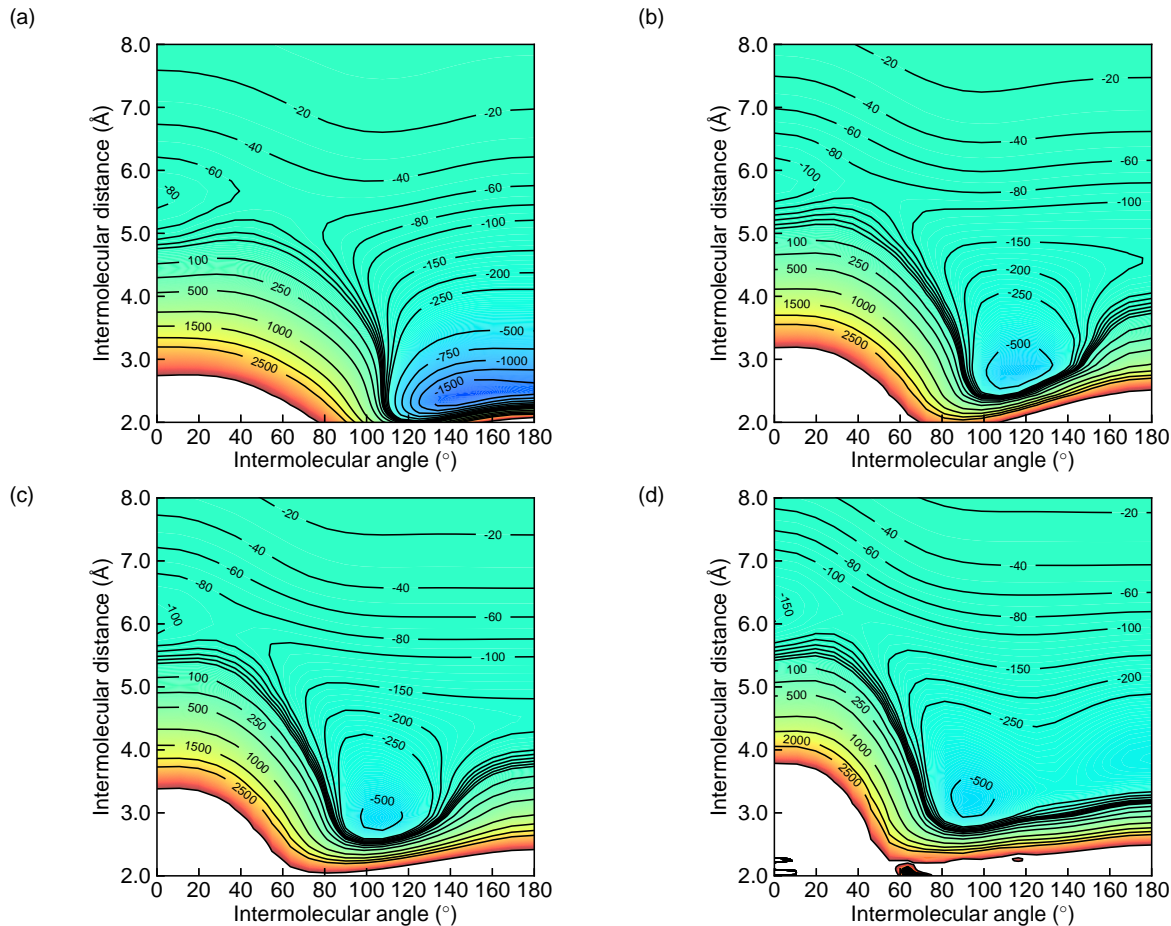


FIG. 1: Nonreactive RCCSD(T)/AVDZ potential energy surfaces between Li and (a) CH_3F , (b) CH_3Cl , (c) CH_3Br , and (d) CH_3I . Contours represent interaction energies in cm^{-1} .

III. RESULTS AND DISCUSSION

A. Nonreactive intermolecular potential energy surfaces for $\text{CH}_3\text{X} + \text{A}$

Potential energy surfaces representing the nonreactive interaction between Li and CH_3F , CH_3Cl , CH_3Br , and CH_3I are shown in Figures 1a to 1d, respectively. The surfaces are constructed at the RCCSD(T)/AVDZ level of theory on a grid of points composed of polar angles θ corresponding to a 21-point Gauss-Lobatto quadrature and a regularly spaced set of 21 intermolecular separations R , forming a grid comprised of 441 points. The polar angles $\theta = 0^\circ$ and $\theta = 180^\circ$ correspond to approach of the Li to the side of the molecule closest to the H-H-H plane and to the halogen atom, respectively. The monomer geometries are held fixed at their experimentally determined equilibrium geometries.⁹³

Two minima are evident on the $\text{CH}_3\text{F} + \text{Li}$ surface in

Figure 1a. The first minimum occurs when Li is positioned at $\theta = 0^\circ$, 6 Å away from the molecular center of mass. The complex has C_{3v} symmetry in this configuration. Given the rather large intermolecular separation and relatively weak attraction ($\sim 100 \text{ cm}^{-1}$), this local minimum may be attributed primarily to induction and dispersion forces. The other minimum is located at $\theta = 140^\circ$, 2.5 Å away from the molecular center of mass. The symmetry of the complex in this orientation is C_s . By symmetry there are actually three minima of this type, each bound by $> 2000 \text{ cm}^{-1}$, making them the global minima. The $\text{CH}_3\text{F} + \text{Li}$ surface exhibits strong anisotropy on the repulsive wall, with the inner turning point rapidly receding by $\sim 2.5 \text{ Å}$ between intermolecular angles of $\theta = 50^\circ$ and $\theta = 100^\circ$. In the region with $\theta > 120^\circ$, the strong covalent attraction responsible for the global minima becomes virtually independent of angle, with a relatively low saddle point occurring at $\theta = 180^\circ$.

The $\text{CH}_3\text{Cl} + \text{Li}$, $\text{CH}_3\text{Br} + \text{Li}$, and $\text{CH}_3\text{I} + \text{Li}$ surfaces are shown in Figures 1b, 1c, and 1d, respectively. The two minima described previously occur at slightly larger intermolecular distances, with the angle θ_e of the C_s minimum being $\sim 20^\circ$ smaller. These surfaces are all qualitatively similar to Figure 1a, except in the region $\theta = 140^\circ$ to 180° . A third minimum appears at $\theta = 180^\circ$ for $\text{CH}_3\text{I} + \text{Li}$: it is located at a similar intermolecular distance and is of comparable depth ($\sim 250 \text{ cm}^{-1}$) to the C_s minimum on the same surface. All geometries included in Figure 1 gave T1 diagnostics⁹¹ not exceeding 0.033, indicating that single-reference RCCSD(T) calculations are expected to be reliable.⁹²

The potential energy surfaces involving the remaining alkali-metal atoms have similar qualitative features for each methyl halide. We therefore focus on quantitative comparisons between key stationary points on the sixteen surfaces. The anisotropy of each surface can be inferred from the interaction energies and geometrical parameters characterizing the stationary points. We consider three stationary points on each surface, one at $\theta = 0^\circ$, one at $\theta = 180^\circ$, and the third at the position of the C_s minimum. By choosing to characterize only a few points on each surface, we are able to perform calculations at a higher level of theory and allow for relaxation of secondary geometrical parameters.

Stationary-point searches using RCCSD(T) are time-consuming and it is more efficient to use RMP2 instead, since it produces similar geometrical parameters for the systems of interest. As a benchmark example we examined the C_s minimum on the fixed-monomer $\text{CH}_3\text{F} + \text{Li}$ surface, where the optimized RCCSD(T)/AVDZ intermolecular parameters are $R = 2.44 \text{ \AA}$ and $\theta = 147.0^\circ$ and the well depth is 1750 cm^{-1} (see Figure 1a). Fixed-monomer optimizations performed using RMP2/AVDZ produced similar values, with R and θ larger by only 0.02 \AA and 0.6° , respectively.

The fixed-monomer approximation is a good one for systems with weak intermolecular forces, but there may be significant monomer distortions if the interactions are comparable to monomer vibrational frequencies. Among the systems of interest here, this effect is most significant for $\text{CH}_3\text{F} + \text{Li}$. When the secondary geometrical parameters were also optimized during the RMP2/AVDZ stationary point search for this system, the C-F bond stretched by 0.03 \AA and the associated R and θ parameters differed from the fixed-monomer RCCSD(T)/AVDZ results by 0.00 \AA and -1.2° , respectively. The RMP2/AVDZ//RCCSD(T)/AVDZ well is 514 cm^{-1} deeper than in the fixed-monomer calculation. We also obtained optimized R and θ parameters using RMP2/AVTZ, which differed from the RCCSD(T)/AVDZ results by -0.03 \AA and 0.1° , respectively. From these tests optimizations at the RMP2/AVDZ level were deemed adequate for our purposes. However, the AVTZ basis set makes a significant difference to the final energetics, so we have used it in the single-point RCCSD(T) calculations.

Interaction energies and geometrical parameters resulting from optimizations at the RMP2/AVDZ//RCCSD(T)/AVTZ level of theory are reported in Table I for all sixteen $\text{CH}_3X + A$ systems. From these results a few trends emerge. For the CH_3F systems, the global minima have C_s geometries and the well depth rises gently from θ_e to 180° . $\text{CH}_3\text{F} + \text{Li}$ and $\text{CH}_3\text{F} + \text{Na}$ have substantially deeper wells than $\text{CH}_3\text{F} + \text{K}$ and $\text{CH}_3\text{F} + \text{Rb}$. Most of the remaining complexes have global minima at C_s geometries, but the preference for this geometry over $\theta = 180^\circ$ decreases from Cl to I, and $\text{CH}_3\text{I} + \text{Na}$ and $\text{CH}_3\text{I} + \text{Rb}$ actually have global minima at $\theta = 180^\circ$. For each of CH_3Cl , CH_3Br and CH_3I , the interactions with Na, K and Rb are comparable but that with Li is substantially stronger.

It is also important to consider the anisotropy around the molecular C_{3v} axis. To investigate this effect in the region of the C_s minimum for $\text{CH}_3\text{F} + \text{Li}$ we have performed an RMP2/AVDZ//RCCSD(T)/AVTZ calculation with the H-C-F-Li dihedral angle constrained to $\phi = 0$. The values $R_e = 2.44$ and $\theta_e = 145.8^\circ$ were obtained, which are identical to those for $\phi = 60^\circ$ (see Table I) and the anisotropy is $\sim 1 \text{ cm}^{-1}$. In the region with $\theta < 145.8^\circ$, the spatial distribution of the hydrogen atoms causes more significant anisotropy about the molecular C_{3v} axis. RMP2/AVDZ//RCCSD(T)/AVTZ calculations were performed to locate the C_s saddle point with $\phi = 60^\circ$ and $\phi = 0$. We find that R_e and θ_e shift from 5.90 \AA and 62.6° at $\phi = 60^\circ$ to 5.67 \AA and 91.7° at $\phi = 0$, indicating that the position of the repulsive wall in this region shifts significantly upon rotation about the molecular C_{3v} axis.

It is useful to compare our results with those for other systems. The value of 2073 cm^{-1} obtained here for the depth of the C_s entrance-channel well in $\text{CH}_3\text{F} + \text{Li}$ is similar to the value of 2100 cm^{-1} obtained for the HF + Li interaction.⁹⁵ Ref. 94 reported well depths for the interactions between various alkali-metal atoms and the NH molecule. For the lowest quartet state at linear A-NH geometries, they are 1799.1 , 651.3 , 784.7 , and 709.3 cm^{-1} for Li, Na, K, and Rb, respectively. For $A + \text{NH}_3$ systems,²⁶ the corresponding well depths for the ground state are 5104 , 2359 , 2161 and 1862 cm^{-1} , respectively. These results follow the trend noted above for the interactions with CH_3Cl , CH_3Br and CH_3I , where the well is similar magnitude for Na, K, and Rb but substantially deeper for Li. The CH_3F systems are rather different, since the wells of $\text{CH}_3\text{F} + \text{K}$ and $\text{CH}_3\text{F} + \text{Rb}$ are similar but those for both $\text{CH}_3\text{F} + \text{Li}$ and $\text{CH}_3\text{F} + \text{Na}$ are considerably deeper.

B. Reactive potential energy surface for $\text{CH}_3\text{Cl} + \text{Li} \rightarrow \text{CH}_3 + \text{LiCl}$

The full potential energy surface for a $\text{CH}_3X + A$ reaction is a hypersurface in 12 dimensions. However, in

TABLE I: Characteristics of selected stationary points on the ground-state nonreactive potential energy surfaces for the $\text{CH}_3X + A$ systems, computed at the RMP2/AVDZ//RCCSD(T)/AVTZ level of theory. Counterpoise-corrected RMP2 energies were used to perform the stationary-point searches. Binding energies (D_e) are reported in cm^{-1} with respect to the energy of infinitely separated geometry-optimized monomers. Intermolecular distances (R_e) and angles (θ_e) are reported in \AA and degrees, respectively.

Alkali-metal atom	$\text{CH}_3\text{F} \cdots A$						$\text{CH}_3\text{Cl} \cdots A$							
	$\theta = 0^\circ$		$\theta = 180^\circ$		C_s minimum		$\theta = 0^\circ$		$\theta = 180^\circ$		C_s minimum			
	D_e	R_e	D_e	R_e	D_e	R_e	θ_e	D_e	R_e	D_e	R_e	θ_e		
Li	78.9	5.90	1852	2.57	2073	2.44	145.8	109.7	6.16	166.1	4.85	846.0	2.79	115.3
Na	61.8	6.31	1815	3.02	1922	2.94	152.7	100.3	6.42	160.8	5.00	312.9	3.83	113.0
K	57.4	6.61	511.2	3.60	644.9	3.42	145.3	65.0	7.13	119.3	5.52	218.5	4.62	111.3
Rb	49.5	6.73	555.3	3.68	585.4	3.58	149.8	55.6	7.12	106.2	5.77	224.2	4.62	111.9
Alkali-metal atom	$\text{CH}_3\text{Br} \cdots A$						$\text{CH}_3\text{I} \cdots A$							
	$\theta = 0^\circ$		$\theta = 180^\circ$		C_s minimum		$\theta = 0^\circ$		$\theta = 180^\circ$		C_s minimum			
	D_e	R_e	D_e	R_e	D_e	R_e	θ_e	D_e	R_e	D_e	R_e	θ_e		
Li	135.0	6.31	259.0	4.46	785.2	2.89	105.0	166.0	6.42	469.4	4.22	663.8	3.23	94.5
Na	127.5	6.51	241.8	4.67	344.1	3.92	102.5	147.7	6.60	416.7	4.47	336.8	4.31	89.9
K	77.3	7.29	190.0	5.21	360.1	4.14	107.7	56.6	7.85	317.3	5.02	376.5	4.31	97.1
Rb	53.7	7.51	152.3	5.60	223.8	4.82	99.3	31.7	7.98	260.1	5.28	182.3	5.23	88.6

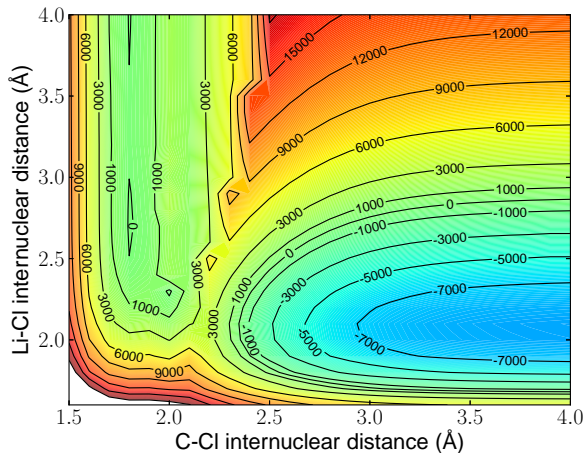


FIG. 2: CASSCF(11,10)/AVDZ potential energy surface for the $\text{CH}_3\text{Cl} + \text{Li}$ reaction as a function of the Li-Cl and C-Cl internuclear coordinates, with the Li-Cl-C angle fixed at 180° and other coordinates optimized. Contours represent interaction energies in cm^{-1} .

many cases a chemical reaction is governed by only a few internal coordinates. In this section we examine low-dimensional cuts through the reactive surface for the model system $\text{CH}_3\text{Cl} + \text{Li}$. Interaction energies were computed at the CASSCF(11,10)/AVDZ level of theory. Figure 2 shows the energy as a function of the Li-Cl and C-Cl internuclear distances, with the Li-Cl-C angle fixed at 180° and other coordinates optimized. Figure 2 shows the entrance and exit channels, as well as the region of the transition state. The entrance channel is centered about the equilibrium CH_3Cl bond distance ($R_{\text{CCl}} \approx 1.8 \text{ \AA}$ for $R_{\text{LiCl}} > 2.3 \text{ \AA}$) and the exit channel is centered about the equilibrium LiCl bond distance ($R_{\text{LiCl}} \approx 2.1 \text{ \AA}$ for $R_{\text{CCl}} > 3.0 \text{ \AA}$). The reac-

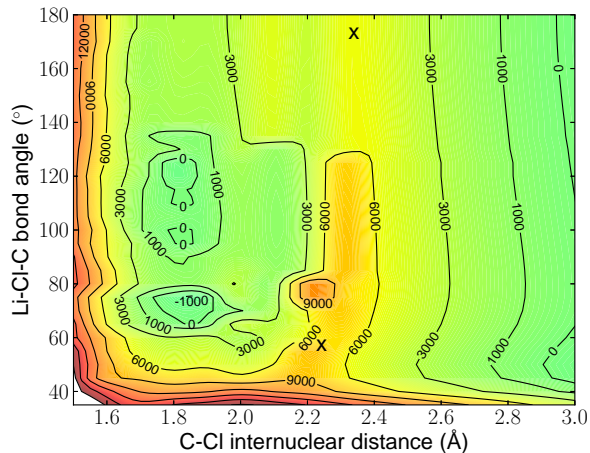


FIG. 3: CASSCF(11,10)/AVDZ potential energy surface for the $\text{CH}_3\text{Cl} + \text{Li}$ reaction as a function of the Li-Cl-C angle and C-Cl internuclear distance, with the Li-Cl distance fixed at 2.75 \AA and other coordinates optimized. Contours represent interaction energies in cm^{-1} .

tion is exothermic, with a late barrier. The transition state is product-like and occurs at $R_{\text{LiCl}} \approx 2.2 \text{ \AA}$ and $R_{\text{CCl}} \approx 2.2 \text{ \AA}$.

In the vicinity of the transition state, there is an avoided crossing between two electronic states of the same symmetry with quite different charge distributions. This causes the ground-state adiabatic wave function to change rapidly when passing through this region and, as a result, geometry optimizations converge toward dissimilar relaxed nuclear configurations on each side of the barrier. There is thus an energy cusp evident where the two geometry-optimized surfaces meet, which is a result of the reduced-dimensionality subspace of optimization parameters we have chosen to work within. The height

of the cusp is a lower bound to the true barrier height. This is because it corresponds physically to the crossing of two segments of the same adiabatic hypersurface which are connected in higher-dimensional space.

Figure 3 shows the interaction energy as a function of the Li-Cl-C bond angle and the C-Cl internuclear distance with the Li-Cl bond distance fixed at 2.75 Å. Here it may be seen that there are actually two low-energy saddle points connecting reactants to products (marked by “X” on Figure 3). The energetically favored angles for reaction span the region $\geq 140^\circ$ near $R_{\text{CCl}} = 2.4$ Å, with the lowest barrier near 180° . This corresponds to the classic rebound reaction. The second pathway near $\theta_{\text{LiClC}} = 60^\circ$ and $R_{\text{CCl}} = 2.3$ Å is steep and narrow, and in fact it appears only if the geometry is optimized at each point during the construction of the potential. This pathway corresponds to insertion of the Li atom into the C-Cl bond. Since its barrier is higher than that for the rebound reaction, we do not consider this pathway further.

If the potential energy surface in Figure 3 is traced along the fixed angle $\theta = 180^\circ$ from $R_{\text{CCl}} = 1.8$ to 3.0 Å, there is a double barrier between reactants and products. In order to investigate whether this phenomenon persists when the potential is computed using higher levels of theory, we have performed CASSCF(3,6)//MS-MR-CASPT2(3,6)/6-31G* calculations with R_{LiCl} fixed at 2.25 Å, θ_{LiClC} fixed at 180° , and R_{CH} and θ_{ClCH} optimized for each point. Five contracted reference states were treated together to obtain a balanced description of the avoided crossings. The resulting potential curves are shown in Figure 4, and shows a series of avoided crossings as a charge-transfer state descends through a series of covalent states with increasing R_{LiCl} . The lowest potential curve shows only one barrier, arising from an avoided crossing with this state. This provides evidence that there is in reality only one barrier to reaction along the cut with $\theta_{\text{LiClC}} = 180^\circ$. It also shows that there is at least one excited state of the collision complex that lies below the energy of $\text{CH}_3\text{Cl} + \text{Li}(^2\text{P})$. Reactions involving excited alkali-metal atoms are in general unlikely to have significant barriers.

C. Reaction profiles and energetics for $\text{CH}_3\text{X} + \text{A} \rightarrow \text{CH}_3 + \text{AX}$

In the previous section we considered $\text{CH}_3\text{Cl} + \text{Li}$ as a model to explore the mechanism of the more general $\text{CH}_3\text{X} + \text{A} \rightarrow \text{CH}_3 + \text{AX}$ DCT reaction. We found that the barrier to reaction is lowest when the alkali-metal atom approaches head-on towards the halogen end of the methyl halide molecule, i.e., with $\theta_{\text{CClLi}} = 180^\circ$. In this section we obtain estimates of the activation energies of all sixteen DCT reactions.

In order to characterize a transition state fully, a saddle point must be located on the PES, characterized by one imaginary vibrational frequency. Despite a lengthy

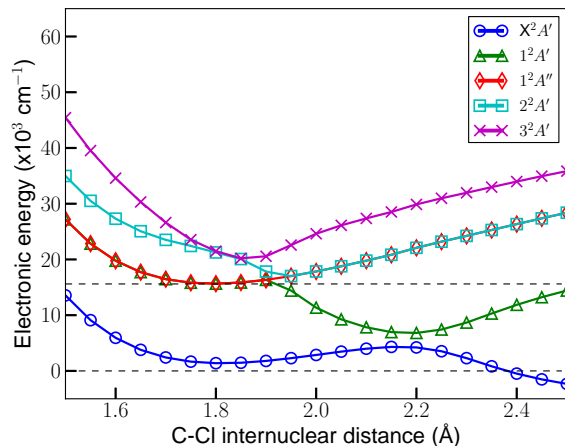


FIG. 4: The five lowest-lying CASSCF(3,6)//MS-MR-CASPT2(3,6)/6-31G* potential energy curves along the C-Cl bond-breaking coordinate for $\text{CH}_3\text{Cl} + \text{Li} \rightarrow \text{CH}_3 + \text{LiCl}$ with R_{LiCl} and θ_{LiClC} fixed at 2.25 Å and 180° , respectively. The two dashed horizontal lines represent the separated reactant energies for $\text{Li}(^2\text{S})$ and $\text{Li}(^2\text{P})$.

effort to locate saddle points for these DCT systems, the searches never converged, and we were forced to develop a less rigorous procedure for estimating the relevant activation energies. We will refer to the quantities generated in this way as “barrier heights” in order to distinguish them from true activation energies.

In our procedure we start from an optimized reactant van der Waals complex and perform constrained optimizations along R_{CX} , incrementally stretching the C-X bond and reoptimizing the secondary geometrical parameters of the complex. The procedure is then repeated, this time starting from the product van der Waals complex and incrementally compressing the C-X bond length while reoptimizing the other geometrical parameters. During these calculations we fix $\theta_{\text{LiClC}} = 180^\circ$, constraining the complex to C_{3v} symmetry. This step-wise procedure is halted in each direction when a calculation fails to converge. Reaction profiles were produced using this procedure at the RMP2//RCCSD(T)/AVDZ level of theory since the MS-MR-CASPT2 method is too expensive for routine calculations when Dunning’s basis sets are employed.

The resulting potential energy curves are shown in Figure 5. We include curves for all four of the systems involving Li to illustrate features common to all 16 reactions studied. The forward and reverse potential energy curve segments can be seen to match fairly well in the region of the transition state. However, for every reaction we examined, only the forward segment yielded a peak. For each system we determined the geometry at a point within $1 \mu\text{Hartree}$ of the peak of the forward potential curve. After this geometry was obtained at the RMP2//RCCSD(T)/AVDZ level of theory, subsequent single-point energy calculations were carried out to ob-

TABLE II: Barrier heights for $\text{CH}_3\text{X} + \text{A} \rightarrow \text{CH}_3 + \text{AX}$ reactions. Structures were located at the RMP2//RCCSD(T)/AVDZ level of theory using a numerical search method, as described in the text. Results of single-point energy calculations performed on the resulting structures are reported below, as computed at the RCCSD(T)/AV x Z level of theory.

Alkali-metal Atom	Basis set level	Methyl halide molecule			
		CH_3F	CH_3Cl	CH_3Br	CH_3I
Li	AVDZ	3728	3026	1163	-249
	AVTZ	4258	3398	1436	-105
	AVQZ	4227	3502	1467	-124
Na	AVDZ	4790	4063	1961	331
	AVTZ	4615	4586	2290	567
	AVQZ	n/c ^a	4743	2309	512
K	AVDZ	6237	3706	2385	1133
	AVTZ	6328	4542	n/c ^a	1151
	AVQZ	6233	5544	n/c ^a	836
Rb	AVDZ	>6000	3810	2584	736
	AVTZ	n/c ^a	n/c ^a	2971	1069
	AVQZ	n/c ^a	n/c ^a	2864	965
Semi-empirical values ^b		15000	4400	2000	200

^aCalculations did not converge.

^bTaken from Ref. 33

tain barrier heights at the RCCSD(T)/AVTZ level of theory.

To confirm that RCCSD(T) gives acceptable energetics in the region of the transition state for these DCT reactions, we have also computed the $\text{CH}_3\text{F} + \text{Li} \rightarrow \text{CH}_3 + \text{LiF}$ reaction profile at the CR-CC(2,3)/VDZ level of theory. Augmented basis functions were not used in these calculations to reduce the computational expense associated with numerical gradients. The CR-CC(2,3)/VDZ reaction profile is also included in Figure 5. Its peak is centered at $R_{\text{CF}} \sim 1.81 \text{ \AA}$ with a reaction barrier height of 3100 cm^{-1} . For comparison, the RMP2//RCCSD(T)/VDZ calculations gives a peak near $R_{\text{CF}} \sim 1.79$ with a reaction barrier height of 3500 cm^{-1} . The two methods give good agreement for the position of the barrier and acceptable agreement ($\sim 500 \text{ cm}^{-1}$) for the barrier height. Keeping the magnitude of this discrepancy in mind, we proceed using RMP2/AVDZ//RCCSD(T)/AV x Z to compute the remaining barrier heights for this class of reactions.

Table II reports barrier heights determined using this procedure for all 16 systems and a variety of basis sets. The $\text{CH}_3\text{X} + \text{A}$ barrier heights mostly increase with increasing alkali-metal atomic number and decrease with increasing halogen atomic number. Some forward calculations involving K and Rb did not reach a peak before failing to converge, so for these cases we provide a lower bound for the height of the barrier. The AVQZ results for Li and Na systems indicate that the AVTZ results are converged to within $\sim 200 \text{ cm}^{-1}$ with respect to the basis-set size. The signs of barrier heights suggest that activation barriers exist for all systems considered here

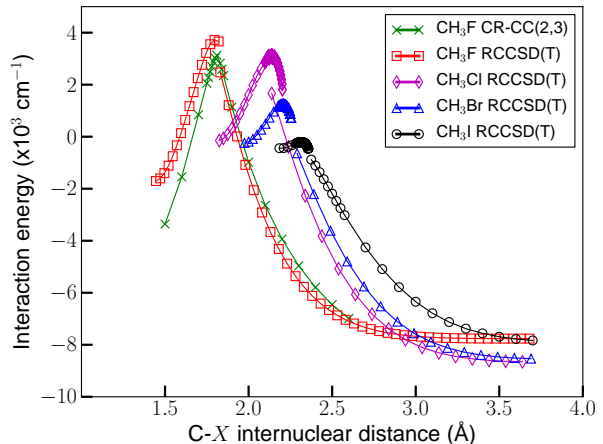


FIG. 5: Reaction profiles for methyl halides CH_3X with Li computed at the RMP2//RCCSD(T)/AVDZ or CR-CC(2,3)/VDZ level of theory. Note that the forward and reverse segments do not match perfectly in the transition state region due to rapid variation of the geometry and charge density as described in the text.

except $\text{CH}_3\text{I} + \text{Li}$, which has a submerged barrier.

The factor that limits the accuracy of the barrier heights presented in Table II is the reliability of the RCCSD(T) method in the region of the transition state. Some of the T1 diagnostics near the peak geometries are as large as ~ 0.10 , indicating that there is significant multi-reference character in these regions. However, since the resulting potential energy curves follow physical trends, we believe that the RCCSD(T) results still give a good estimate of the barrier heights. A preliminary benchmark study comparing RCCSD(T) with multireference configuration interaction calculations for the related DEA reaction of CH_3F suggests that the error in the RCCSD(T) activation barriers might be as large as $\sim 1000 \text{ cm}^{-1}$. We therefore cannot be certain that barriers exist for any of the four $\text{CH}_3\text{I} + \text{A}$ reactions.

Finally, it is interesting to compare our barrier heights with the values obtained by Wu from the analogous dissociative electron attachment processes. These are included in the bottom row of Table II. Wu's estimates are in reasonably good agreement with ours for systems involving CH_3Cl , CH_3Br , and CH_3I . The DEA approach slightly underestimates activation barriers for systems involving Li and overestimates barriers for systems involving Na to Rb. For systems involving CH_3F , Wu's estimated reaction barriers are 2 to 3 times larger than the values we obtain. This large discrepancy is probably attributable to the significant stabilization of the product-like transition state by the presence of the alkali-metal atom.

IV. CONCLUSIONS AND FUTURE OUTLOOK

We have investigated both nonreactive and reactive potential energy surfaces for interaction of methyl halides with alkali-metal atoms. Reactive collisions occurring at cold and ultracold temperatures can usually proceed only if there is an exothermic reaction pathway with a submerged or nonexistent barrier. Of the 16 reactant combinations considered in this study, submerged barriers are likely to be present only for the $\text{CH}_3\text{I} + \text{Li}$ reactions, though they cannot be ruled out for CH_3I with heavier alkali-metal atoms. For the remaining 12 atom-molecule combinations, significant barriers to reaction are predicted.

For the nonreactive interactions between methyl halides and alkali-metal atoms, we find deep minima and strong anisotropies in the well region for all systems con-

sidered. Systems involving Li have especially strong and anisotropic interactions, but collision systems involving Li will also have larger centrifugal barriers than for other alkali-metal atoms and these may suppress cold inelastic collisions. In future work we will investigate the nonreactive surfaces in greater detail and explore the extent to which centrifugal barriers suppress inelastic collisions of trapped methyl halide molecules with ultracold Li atoms.

Acknowledgments

We are grateful to Heather Lewandowski for discussions that identified this problem and to the Engineering and Physical Sciences Research Council for funding under grant no. EP/I012044/1.

-
- ¹ R. V. Krems, *Phys. Chem. Chem. Phys.* **10**, 4079 (2008).
 - ² B. C. Regan, E. D. Commins, C. J. Schmidt, and D. DeMille, *Phys. Rev. Lett.* **88**, 071805 (2002).
 - ³ J. J. Hudson, B. E. Sauer, M. R. Tarbutt and E. A. Hinds, *Phys. Rev. Lett.* **89**, 023003 (2002).
 - ⁴ J. van Veldhoven, J. Küpper, H. L. Bethlem, B. Sartakov, A. J. A. van Roij and G. Meijer, *Eur. Phys. J. D* **31**, 337 (2004).
 - ⁵ T. Zelevinsky, S. Blatt, M. M. Boyd, G. K. Campbell, A. D. Ludlow and J. Ye, *ChemPhysChem*. **9**, 375 (2008).
 - ⁶ J. D. Weinstein, R. deCarvalho, T. Guillet, B. Friedrich, and J. M. Doyle, *Nature* **395**, 148 (1998).
 - ⁷ H. L. Bethlem and G. Meijer, *Int. Rev. Phys. Chem.* **22**, 73 (2003).
 - ⁸ N. Vanhaecke, U. Meier, M. Andrist, B. H. Meier, and F. Merkt, *Phys. Rev. A* **75**, 031402 (2007).
 - ⁹ S. D. Hogan, D. Sprecher, M. Andrist, N. Vanhaecke, and F. Merkt, *Phys. Rev. A* **76**, 023412 (2007).
 - ¹⁰ E. Narevicius, C. G. Parthey, A. Libson, J. Narevicius, I. Chavez, U. Even, and M. G. Raizen, *New J. Phys.* **9**, 358 (2007).
 - ¹¹ E. S. Shuman, J. F. Barry, and D. DeMille, *Nature* **467**, 820 (2010).
 - ¹² P. Soldán and J.M. Hutson, *Phys. Rev. Lett.* **92**, 163202 (2004).
 - ¹³ B. K. Stuhl, M. T. Hummon, M. Yeo, G. Quéméner, J. L. Bohn, and J. Ye, *Nature* **492**, 396 (2012).
 - ¹⁴ A. Volpi and J. L. Bohn, *Phys. Rev. A* **65**, 052712 (2002).
 - ¹⁵ M. Zeppenfeld, B. G. U. Englert, R. Glöckner, A. Prehn, M. Mielenz, C. Sommer, L. D. van Buuren, M. Motsch, and G. Rempe, *Nature* **491**, 570 (2012).
 - ¹⁶ J. M. Hutson and P. Soldán, *Int. Rev. Phys. Chem.* **25**, 497 (2006).
 - ¹⁷ K. M. Jones, E. Tiesinga, P. D. Lett, and P. S. Julienne, *Rev. Mod. Phys.* **78**, 483 (2006).
 - ¹⁸ T. Köhler, K. Góral, and P. S. Julienne, *Rev. Mod. Phys.* **78**, 1311 (2006).
 - ¹⁹ H. L. Bethlem, G. Berden, and G. Meijer, *Phys. Rev. Lett.* **83**, 1558 (1999).
 - ²⁰ H. L. Bethlem, G. Berden, F. M. H. Crompvoets, R. T. Jongma, A. J. A. van Roij and G. Meijer, *Nature* **406**, 491 (2000).
 - ²¹ J. R. Bochinski, E. R. Hudson, H. J. Lewandowski, G. Meijer and J. Ye, *Phys. Rev. Lett.* **91**, 243001 (2003).
 - ²² J. J. Hudson, B. E. Sauer, M. R. Tarbutt and E. A. Hinds, *Phys. Rev. Lett.* **89**, 023003 (2002).
 - ²³ E. R. Hudson, C. Ticknor, B. C. Sawyer, C. A. Taatjes, H. J. Lewandowski, J. R. Bochinski, J. L. Bohn and J. Ye, *Phys. Rev. A* **73**, 063404 (2006).
 - ²⁴ S. Jung, E. Tiemann and C. Lisdat, *Phys. Rev. A* **74**, 040701 (2006).
 - ²⁵ S. Y. T. van de Meerakker, I. Labazan, S. Hoekstra, J. Küpper and G. Meijer, *J. Phys. B* **39**, S1077 (2006).
 - ²⁶ P. S. Żuchowski and J. M. Hutson, *Phys. Rev. A* **78**, 022701 (2008).
 - ²⁷ P. S. Żuchowski and J. M. Hutson, *Phys. Rev. A* **79**, 062708 (2009).
 - ²⁸ L. P. Parazzoli, N. J. Fitch, P. S. Żuchowski, J. M. Hutson, and H. J. Lewandowski, *Phys. Rev. Lett.* **106**, 193201 (2011).
 - ²⁹ D. Lian-Zhong, F. Guang-Bin, and Y. Jian-Ping, *Chinese Phys. B* **18** 0149 (2009).
 - ³⁰ *Alkali Halide Vapors*, edited by P. Davidovits and D. L. McFadden, (Academic, New York, 1979).
 - ³¹ X. Y. Chang, R. Ehlich, A. J. Hudson, J. C. Polanyi, and J.-X. Wang, *J. Chem. Phys.* **106**, 3988 (1997).
 - ³² A. J. Hudson, F. Y. Naumkin, H. Oh, J. C. Polanyi and S. A. Raspopov, *Faraday Discuss.* **118**, 191 (2001).
 - ³³ K. T. Wu, *J. Phys. Chem.* **83**, 1043 (1979).
 - ³⁴ M. Hotokka, B. O. Roos, and L. Ebersson, *J. Chem. Soc. Perkin Trans. II* **12**, 1979 (1986).
 - ³⁵ J. Bertran, I. Gallardo, M. Moreno, J.-M. Savéant, *J. Am. Chem. Soc.* **114**, 9576 (1992).
 - ³⁶ P. Piecuch, *J. Mol. Struct.* **437**, 503 (1997).
 - ³⁷ R. Benassi, F. Bernardi, A. Bottoni, M. A. Robb, and F. Taddei, *Chem. Phys. Lett.* **161**, 79 (1989).
 - ³⁸ A. Soriano, E. Silla, and I. Tuñón, *J. Chem. Phys.* **116**, 6102 (2002).
 - ³⁹ D. Ajitha, M. Wierzbowska, R. Lindh, and P. A. Malmqvist, *J. Chem. Phys.* **121**, 5761 (2004).
 - ⁴⁰ P. R. Brooks, *J. Chem. Phys.* **50**, 5031 (1969).

- ⁴¹ G. Marcelin and P. R. Brooks, *J. Am. Chem. Soc.* **97**, 1710 (1975).
- ⁴² P. R. Brooks, *Science* **193**, 11 (1976).
- ⁴³ P. R. Brooks, J. S. McKillop, and H. G. Pippin, *Chem. Phys. Lett.* **66**, 144 (1979).
- ⁴⁴ P. R. Brooks, P. W. Harland, L. F. Phillips, and H. S. Carman, *J. Phys. Chem.* **96**, 1557 (1992).
- ⁴⁵ R. J. Beuhler and R. B. Bernstein, *J. Chem. Phys.* **51**, 5305 (1969).
- ⁴⁶ D. H. Parker, K. K. Chakravorty, and R. B. Bernstein, *J. Phys. Chem.* **85**, 466 (1981).
- ⁴⁷ D. H. Parker, K. K. Chakravorty, and R. B. Bernstein, *Chem. Phys. Lett.* **86**, 113 (1982).
- ⁴⁸ R. B. Bernstein, *J. Chem. Phys.* **82**, 3656 (1985).
- ⁴⁹ D. H. Parker and R. B. Bernstein, *Annu. Rev. Phys. Chem.* **40**, 561 (1989).
- ⁵⁰ S. R. Gandhi and R. B. Bernstein, *J. Chem. Phys.* **93**, 4024 (1990).
- ⁵¹ S. Stolte, *Ber. Bunsenges. Phys. Chem.* **86**, 413 (1982).
- ⁵² S. Stolte, in *Atomic and Molecular Beam Methods*, edited by G. Scoles (Oxford: Oxford University Press), Volume 1, Chapter 25, pp. 631-652.
- ⁵³ M. H. M. Janssen, D. H. Parker, and S. Stolte, *J. Phys. Chem.* **95**, 8142 (1991).
- ⁵⁴ J. Bulthuis and S. Stolte, *J. Phys. Chem.* **95**, 8180 (1991).
- ⁵⁵ J. Bulthuis, J. B. Milan, M. H. M. Janssen, and S. Stolte, *J. Chem. Phys.* **94**, 7181 (1991).
- ⁵⁶ H. J. Loesch and A. Remscheid, *J. Phys. Chem.* **95**, 8194 (1991).
- ⁵⁷ J.-M. Mestdagh, B. Soep, M.-A. Gaveau, and J.-P. Visticot, *Int. Rev. Phys. Chem.* **22**, 285 (2003).
- ⁵⁸ A. E. Wiskerke, S. Stolte, H. J. Loesch, and R. D. Levine, *Phys. Chem. Chem. Phys.* **2**, 757 (2000).
- ⁵⁹ P. J. Knowles, C. Hampel, and H.-J. Werner, *J. Chem. Phys.* **99**, 5219 (1993).
- ⁶⁰ J. D. Watts, J. Gauss and R. J. Bartlett, *J. Chem. Phys.* **98**, 8718 (1993).
- ⁶¹ H.-J. Werner and P. J. Knowles, *J. Chem. Phys.* **82**, 5053 (1985).
- ⁶² P. J. Knowles and H.-J. Werner, *Chem. Phys. Lett.* **115**, 259 (1985).
- ⁶³ G. R. Magoon, J. Aguilera-Iparraguirre, W. H. Green, J. J. Lutz, P. Piecuch, H. W. Wong, and O. O. Oluwole, *Int. J. Chem. Kinet.* **44**, 179 (2012).
- ⁶⁴ H.-J. Werner, *Mol. Phys.* **89**, 645 (1996).
- ⁶⁵ J. Finley, P. Å. Malmqvist, B. O. Roos, L. Serrano-Andrés, *Chem. Phys. Lett.* **288**, 299 (1998).
- ⁶⁶ B. O. Roos and K. Andersson, *Chem. Phys. Lett.* **245** 215 (1995).
- ⁶⁷ P. Piecuch and M. Włoch, *J. Chem. Phys.* **123**, 224105 (2005).
- ⁶⁸ P. Piecuch, M. Włoch, J. R. Gour, and A. Kinal, *Chem. Phys. Lett.* **418**, 463 (2005).
- ⁶⁹ M. Włoch, M. D. Lodriguito, P. Piecuch, and J. R. Gour, *Mol. Phys.* **104**, 2149 (2006).
- ⁷⁰ M. Włoch, J. R. Gour, and P. Piecuch, *J. Phys. Chem. A* **111**, 11359 (2007).
- ⁷¹ J. J. Zheng, J. R. Gour, J. J. Lutz, M. Włoch, P. Piecuch, and D. G. Truhlar, *J. Chem. Phys.* **128**, 044108 (2008).
- ⁷² Y. Zhao, O. Tishchenko, J.R. Gour, W. Li, J.J. Lutz, P. Piecuch, and D. G. Truhlar, *J. Phys. Chem. A* **113**, 5786 (2009).
- ⁷³ P. Piecuch, J. R. Gour, and M. Włoch, *Int. J. Quantum Chem.* **108**, 2128 (2008).
- ⁷⁴ P. Piecuch, J. R. Gour, and M. Włoch, *Int. J. Quantum Chem.* **109**, 3268 (2009).
- ⁷⁵ T. H. Dunning, *J. Chem. Phys.* **90**, 1007 (1989).
- ⁷⁶ R. A. Kendall, T. H. Dunning, and R. J. Harrison, *J. Chem. Phys.* **96**, 6796 (1992).
- ⁷⁷ W. J. Hehre, R. Ditchfield, and J. A. Pople, *J. Chem. Phys.* **56**, 2257 (1972).
- ⁷⁸ J. D. Dill and J. A. Pople, *J. Chem. Phys.* **62**, 2921 (1975).
- ⁷⁹ P. C. Hariharan and J. A. Pople, *Theoret. Chimica Acta* **28**, 213 (1973).
- ⁸⁰ M. M. Francl, W. J. Pietro, W. J. Hehre, J. S. Binkley, M. S. Gordon, D. J. DeFrees and J. A. Pople, *J. Chem. Phys.* **77**, 3654 (1982).
- ⁸¹ I. S. Lim, P. Schwerdtfeger, B. Metz, and H. Stoll, *J. Chem. Phys.* **122**, 104103 (2005).
- ⁸² K. A. Peterson, D. Figgen, E. Goll, H. Stoll, M. Dolg, *J. Chem. Phys.* **119**, 11113 (2003).
- ⁸³ K. A. Peterson, B. C. Shepler, D. Figgen, and H. Stoll, *J. Phys. Chem. A* **110**, 13877 (2006).
- ⁸⁴ S. F. Boys and F. Bernardi, *Mol. Phys.* **19**, 553 (1970).
- ⁸⁵ S. Sekušak and A. Sabljčić, *J. Comp. Chem.* **18** 1190 (1997).
- ⁸⁶ MOLPRO, version 2012.1, a package of *ab initio* programs, H.-J. Werner, P. J. Knowles, G. Knizia, F. R. Manby, M. Schtz, and others, see <http://www.molpro.net>.
- ⁸⁷ M. W. Schmidt, K. K. Baldrige, J. A. Boatz, S. T. Elbert, M. S. Gordon, J. H. Jensen, S. Koseki, N. Matsunaga, K. A. Nguyen, S. Su, T. L. Windus, M. Dupuis, and J. A. Montgomery, *J. Comput. Chem.*, **14**, 1347 (1993).
- ⁸⁸ M. S. Gordon and M. W. Schmidt, in "Theory and Applications of Computational Chemistry: the first forty years" C. E. Dykstra, G. Frenking, K. S. Kim, and G. E. Scuseria (editors), pp 1167, Elsevier, Amsterdam, 2005.
- ⁸⁹ K. L. Schuchardt, B. T. Didier, T. Elsethagen, L. Sun, V. Gurumoorthi, J. Chase, J. Li, T. L. and Windus, *J. Chem. Inf. Model.*, **47**, 1045 (2007).
- ⁹⁰ H. Stoll, *Pseudopotentials, ECP*, <http://www.theochem.uni-stuttgart.de/pseudopotentials/index.en.htm>
- ⁹¹ T. J. Lee and P. R. Taylor, *Int. J. Quant. Chem.* **23**, 199 (1989).
- ⁹² J. C. Rienstra-Kiracofe, W. D. Allen, and H. F. Schaefer, *J. Phys. Chem. A* **104**, 9823 (2000).
- ⁹³ CRC Handbook of Chemistry and Physics, edited by D. R. Lide, 81st edition (CRC, New York, 2000-2001).
- ⁹⁴ P. Soldán, P. S. Żuchowski, and J. M. Hutson, *Faraday Discuss.* **142**, 191 (2009).
- ⁹⁵ Q. Fan, H. Li, H. Feng, W. Sun, T. Lu, A. C. Simmonett, Y. Xie, and H. F. Schaefer, III, *J. Phys. Chem. A*, **117**, 10027 (2013).